MATERIALE PLASTICE
https://revmaterialeplastice.ro
https://doi.org/10.37358/Mat.Plast.1964

Piezoelectric thin Film Composites with $BaTiO_3$ for Microelectronics

MIHAELA ARADOAEI[1], ANDREEA MARIA LUCACI[1], ROMEO CRISTIAN CIOBANU[1], CRISTINA SCHREINER[1], BOGDAN-GEORGE RUSU[2], GABRIELA ELENA HITRUC[2], MAGDALENA AFLORI[2], MARIUS PAULET[1], ALINA RUXANDRA CARAMITU[3], ADRIANA MARIANA BORS[4*]

[1] Gheorghe Asachi Technical University, Department of Electrical Measurements and Materials, 67 Profesor Dimitrie Mangeron Blvd., 700050, Iasi, Romania
[2] Institute of Macromolecular Chemistry "Petru Poni", 41A Grigore Ghica Vodă Str., 700487, Iasi, Romania
[3] National Institute for Research and Development in Electrical Engineering ICPE - CA Bucharest, 313 Splaiul Unirii, 030138, Bucharest, Romania
[4] Research Institute for Hydraulic and Pneumatics (INOE 2000 - IHP) from Bucharest, Branch of the National Research and Development Institute for Optoelectronics - INOE 2000, 14 Cutitul de Argint Str., 0400558, Bucharest, Romania

Abstract: *The piezocomposites from poly-(vinylidene fluoride) (PVDF) with $BaTiO_3$ (BT) are largely presented in literature, but the composites from polydimethylsiloxane (PDMS) with BT consist a very new scientific preoccupation. The novelty of the paper lies in a new simpler route of preparation of the two composites with PDMS and respectively PVDF matrix, with tailored deposition on specific substrates for microelectronic use (e.g. indium-tin-oxide ITO/glass, Si/Pt, polyethylene terephthalate PET), along with an extensive comparation of their dielectric features, a consistent comparison of the influence of polymer matrix upon the piezoelectric features, and a demonstration of direct use for microelectronic applications of the composites of BT with PDMS. An interesting effect is observed around 100 kHz domain, determined by the activity and architecture of BT particles mainly for the BT-PDMS composites, which induce an additional ionic-dipolar conjugated polarization, as a displacement due to the balance between the resonance and anti-resonance frequency. Such phenomena explain the potential use of such composites as resonators/filters, and BT-PDMS composites should be further investigated for tailored applications in radiofrequency electronic field. We can appreciate that superior piezoelectric features are offered by the composites of BT with PDMS, comparing to the composites with PVDF, which means that the composites of BT with PDMS were worth to study, leading to more versatile variants of electronic characteristics and with superior values.*

Keywords*: polyvinylidene fluoride; polydimethylsiloxane; barium titanate, piezoelectric thin film composites, dielectric characteristics, piezoelectric sensors, energy harvesting devices*

1. Introduction

Piezoelectricity, which refers to stress-induced electricity, is derived from the Greek words "piezein," which means "to press," and "lektron," which means "amber" [1]. The piezoelectric result characterizes a material's capacity to develop opposing electrical charges that are spatially separated in response to mechanical deformation brought on by an external force [1]. An electric dipole or piezo-potential is created when electrical charges of different polarities are generated at opposite sides of a single piece of deformed material. Inorganic piezoelectric ceramics-based alternative approaches for piezoelectric materials and composites have been proposed [2], including lead-free inorganic materials like $(Na,K)NbO_3$ [3] and organic polymer hybrids, including PHB/PANi [4]. In comparison to inorganic materials, polymer-based piezoelectric materials, like PVDF or its copolymer poly-(vinylidene fluoride)-trifluoroethylene (PVDF-TrFE), have a number of distinct advantages, including good mechanical flexibility, ease of molding, chemical stability, and biocompatibility [5]. The ferroelectric, piezoelectric, pyroelectric, and enhanced dielectric characteristics of these polymers make them multifunctional [6-8].

**email: bors.ihp@fluidas.ro*

A piezoelectric polymer's degree of crystallinity affects the d33 piezoelectric response, which rises with crystallinity [9], enabling for higher piezoelectric potential values to be attained. A PVDF harvester, for instance, delivered an average output power of 1mW while moving at a frequency of about 1Hz [10]. By adjusting the direction of the applied force, it is possible to tailor the output power produced by altering the quantity and direction of the strain that is created in a PVDF film.

By adjusting the direction of the applied force, it is possible to tailor the output power produced by altering the quantity and direction of the strain that is created in a PVDF film. When an input force of 4 N (2 Hz) was applied at angles of 0°, 45°, and 90°, respectively, the harvester's greatest output peak voltages were measured to be 1.75, 1.29, and 0.98 V; the corresponding maximum output power values were 0.064, 0.026, and 0.02 W. The harvester also produced a consistent output voltage for 1.4 104 cycles and effectively detected and converted strain energy - a multidirectional input force produced by different human motions - into electrical energy [11].

The well-known dielectric ceramic barium titanate BT has relevant piezoelectric coefficients (d33) along the [001] and [111] orientations of the perovskite cubic crystal, respectively, of 90 and 190 pC/N [12]. Due to its distinctive properties, which include excellent piezoelectric and ferroelectric properties, catalysis, optical, and photoluminescence properties, BT has found a wide range of applications for use in high dielectric capacitors and energy storage devices [13-17], transducers [18-20], actuators [21,22], flexible piezoelectric sensors [23-26], and nanogenerators, electro-optic sensors, photocatalysts. Particularly, BT has been widely used as a dielectric material in ceramic capacitors due to its dielectric properties. At ambient temperature, the dielectric constant (r) of BT may reach as high as 7000, and it reaches its maximum values across a limited temperature range close to the Curie temperature, which is between 120 and 130 C [26]. Kuo et al. [27-29] also found a very high value of 25,000 for sintered BT ceramic at room temperature. It has been discovered that the dielectric characteristics of BT depend on the grain size [30-32]. When the grain size is more than 200 nm, the reported dielectric constant of BT in the literature [33-35] ranges from 1000 to 5000. The dielectric permittivity falls as the particle size does. Hoshina [36-40] shown that the dielectric constant of BT ceramic reduces from 8000 to around 600 when the grain size is reduced from 1.1 m to 20 nm.

BT is a potential nucleating filler for PVDF-based composites since it is simple to prepare and can have its chemical composition precisely controlled. Recently, several authors [41-44] have shown how PVDF/BT nanocomposites have better dielectric and piezoelectric properties. The bulk of research have demonstrated that electrospun PVDF/BT fiber mats and solution-cast films have higher dielectric constants, which leads to higher electric energy densities [45, 46]. Flexible energy harvesting devices with good performance and a high current output were created using PVDF loaded with BT nanowires that were 4 m long and 150 nm wide [45]. According to a recent research, the piezoelectric coefficient rose with the weight percentage of the nanofiller, reaching a value of up to 130 p.m./V at a 20 weight percent loading of BT NPs in an electrospun PVDF scaffold [45].

In this work, the effects of the presence of various lead-free components in the structure of the piezoelectric polymers on their piezo-response or energy-harvesting performance are presented. The piezocomposites described are mostly based on poly-(vinylidene fluoride) (PVDF), and polydimethyl-siloxane (PDMS), loaded with inorganic compounds nanofillers of barium titanate $BaTiO_3$. Even if the composites from PVDF with BT are largely presented in literature in the past, they come again in actuality for certain application, e.g. [46, 47], and the composites from PDMS with BT consist a very new scientific preoccupation e.g. [48-51], with only few studies upon their features. The innovation presented in the paper lies in a new simpler route of preparation of the two composites with PDMS and respectively PVDF matrix, with tailored deposition on specific substrates for microelectronic use (e.g. indium-tin-oxide ITO/glass, Si/Pt, polyethylene terephthalate PET), along with an extensive comparation of their dielectric features, a consistent comparison of the influence of polymer matrix upon the piezoelectric polarization characteristics, and a demonstration of direct use for microelectronic applications of the composites of BT with PDMS.

2. Materials and methods

2.1. Synthesis procedures

Two types of composite films were made from thermoplastic polymer matrix: polyvinylidene fluoride (PVDF) and respectively polydimethylsiloxane (PDMS), doped with tetragonal $BaTiO_3$ (BT) particles of irregular shape (< 2µm dimension) from Sigma Aldrich, with 2 concentrations for each composite type (30% and 70% $BaTiO_3$).

The preparation of the PVDF-BT composite is presented in Figure 1 and involves a first step of mixing PVDF in dimethylformamide with a ratio of 1:1, adding BT by ultrasonic mixing until homogenization (light mixing for approximatively 2h), depositing in a Petri dish and pre-drying the mixture at 100ºC for approximatively 1-2 h, then depositing the film by spin-coating at 1000-1500 rpm on a certain support and drying the film at 80ºC.

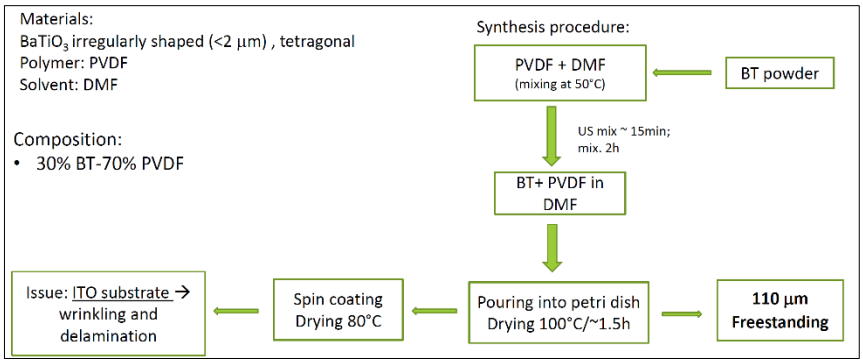

Figure 1. Synthesis process for PVDF-BT composites

The preparation of the PDMS-BT composite is presented in Figure 2 and involves an ultrasonic mixing step of PDMS in benzene with a ratio of 1:2, the addition of BT with light mixing for about 10h, the subsequent addition of PDMS in benzene in a ratio of 1:2 until homogenization, final ultrasonic mixing of the mixture, film deposition by spin-coating on a certain support at 1000-1500 rpm and drying of the film at 80ºC.

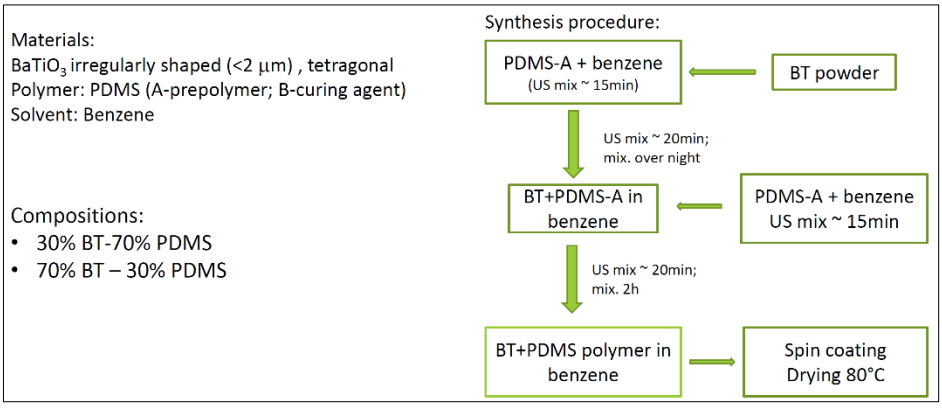

Figure 2. Synthesis process for PDMS-BT composites

More samples on different support (ITO/glass, Si/Pt and PET- the last one being used for extracting freestanding films too) were manufactured, with different thicknesses, to test their features in order to potentially become successful candidates for microelectronic applications with, or without support.

2.2. Characterization equipment

- SEM optical scanning microscopy were performed with a field emission and focused ion beam scanning electron microscope (SEM) model Tescan Lyra III XMU (Libušina tř. 21 623 00, Brno—Kohoutovice, Czech Republic).

- Fourier transform infrared spectra of composites were recorded with a Vertex 70, Bruker, using the Attenuated Total Reflection (ATR) module, equipped with a single reflection diamond crystal at an angle of 45º. To improve the signal/noise ratio a number of 64 accumulations per spectrum was recorded, with standard spectral range: 370-7500 cm^{-1}, far IR extension: 50-680 cm^{-1}, resolution: 2 cm^{-1}.

- Dielectric features were determined by using the Broadband Dielectric Spec-trometer (Novocontrol GMBH) encompassing an Alpha frequency response an-alyzer and Quattro temperature controller with tailored measurement cells. The manufactured samples where sandwiched between two copper electrodes of 20 mm diameter and placed inside the temperature-controlled cell [52].

- The piezoelectric features were measured by using an Aixact TF Analyzer 2000 - Electric Hysteresis Curve Lift System (static and dynamic hysteresis); the volt-age that can be applied to the sample is +/- 100V to +/- 10kV).

The hysteresis curves were raised starting with the frequency of 0.1 Hz, at an electric voltage 20% lower than the breakdown voltage of the samples. Simultaneously, the displacement of the sample can be measured, with a laser interferometry system.

3. Results and discussions

3.1. SEM structural analyses for $BaTiO_3$

SEM pictures and XRD analysis for $BaTiO_3$ powders are presented in Figure 3.

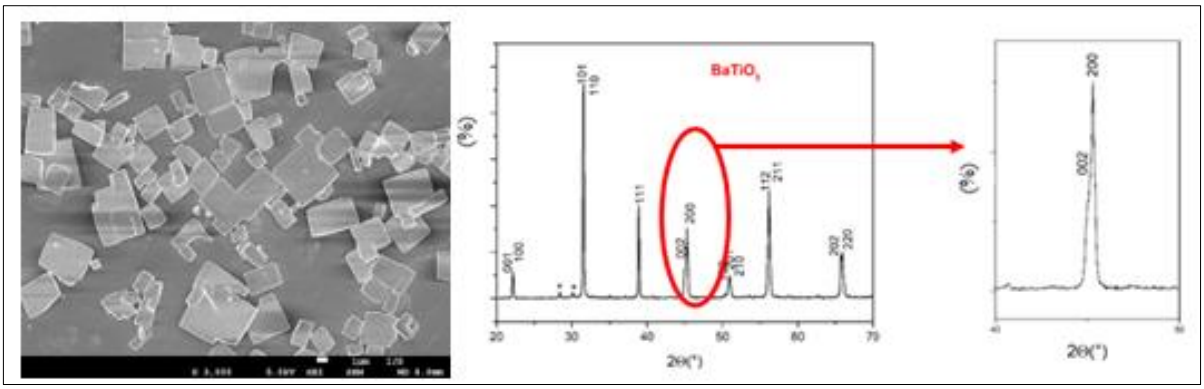

Figure 3. Structural analysis for $BaTiO_3$ powders

Quasi-cube-like particles were noticed, most likely formed due to Volmer Weber growth procedure at manufacturer. According to the XRD in Figure 3, in which no clear tetragonal splitting was observed, the $BaTiO_3$ cube particles do not exhibit high tetragonality. The sight asymmetry of the XRD diffraction line at 2Θ45° indicates that the crystal structure is also not fully cubic.

3.2. Fourier transform infrared spectra

In Figure 4 the FTIR spectrum of polydimethylsiloxane doped with $BaTiO_3$ (30%) is presented. Vibrations located at 2904 and 2963 cm^{-1} can be noticed, attributed to the symmetric and asymmetric νC – H vibrations found in $-CH_3$ and in $Si-CH_3$ [53]. The absorption band around 1259 cm^{-1} is the main band that characterizes δC – H methyl groups bonded to silicon. The absorption bands in the range of 1000-1109 cm^{-1} are attributed to the νSi - O - Si vibrations found in the siloxane matrix. Broad bands of the νOH vibration are observed in the 3000-3500 cm^{-1} region.

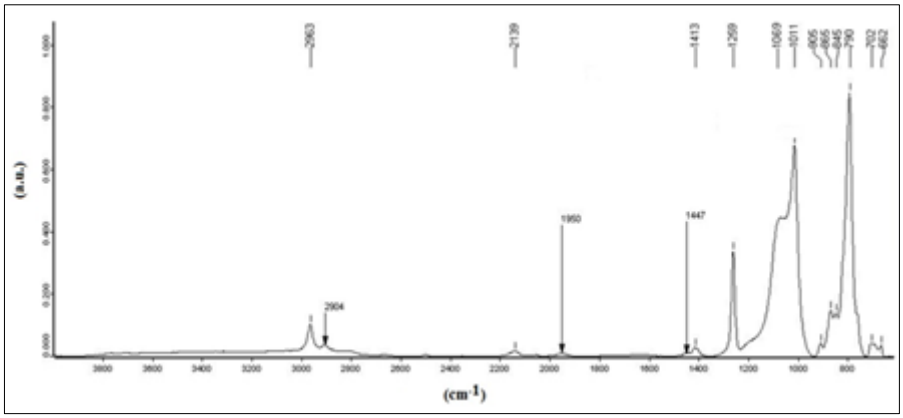

Figure 4. FTIR spectrum of polydimethylsiloxane doped with $BaTiO_3$ (30%)

On the other hand, specific vibrations of PDMS films located at 860 and 792 cm^{-1}, are noticed, attributed to δSi-CH_3 vibrations and also νSi-C vibrations are observed, at 1400 and 1259 cm^{-1} - symmetric and asymmetric vibrations of δCH_3 in Si-CH_3 groups [54]. The vibrations at 1080 and 1015 cm^{-1} are assigned to νSi - O - Si, corresponding to specific vibrations in PDMS.

Multicomponent bands of νSi-O-Si vibrations for PDMS were highlighted in the range between 900 and 1200 cm^{-1}. The peak at 1100 cm^{-1} corresponds to the νSi-O vibration and the Si-C and δ $Si(CH_3)_2$ bands appear in the region 825-865 cm^{-1} and 785–815 cm^{-1}. The significant difference in the FTIR spectrum is observed between a pure PDMS polymer and the filler-doped one in the spectrum, through the vibration located at 905 cm^{-1}, and we are certain that the sample also contains barium titanate in interaction with the PDMS polymer [55].

Figures 5 presentes the FTIR spectra of polyvinylidene fluoride (PVDF) films doped with $BaTiO_3$ at the concentrations of 30%.

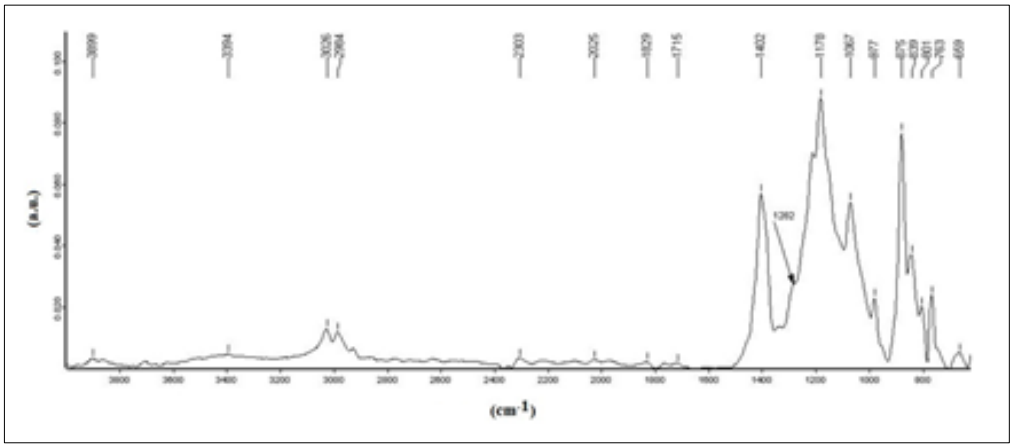

Figure 5. FTIR spectrum of polyvinylidene fluoride doped with $BaTiO_3$ (30%)

Here the bands located at 3025 and 2983 cm^{-1} correspond to νCH_2 as asymmetric and symmetric vibrations in PVDF. The absorption vibrations appearing at 1401 and 1403 cm^{-1} respectively for PVDF-30% and PVDF-70% were attributed to the ωCH_2 vibration. The νC-C vibration in PVDF was located at 1185 cm^{-1} [56] and those at 878 and 840 cm^{-1} were attributed to the ν-asymmetric C - C - C and νCF vibrations of PVDF [57].

There is still no clear information on how the amorphous part of PVDF may influence the FTIR spectra. Therefore, the discussion was focused on the crystalline phase, particularly the most common α, β, and γ crystallization forms. The FTIR spectrum indicated a strong α-form of crystallization. In particular, there are two intense bands located at 763 and 614 cm^{-1} (characteristic for α-form) with a weak vibration at 1283 cm^{-1} which is exclusively for the β phase. Therefore, it can be concluded that a

strong α crystallization with some presence of β form are coexisting in the PVDF film, by the presence of vibrations located at 1283, 837 and 839 cm^{-1} respectively. The presence of β-crystallization is identified in infrared spectroscopy mainly by the characteristic absorption band at 840 cm^{-1} and in the case of the α-PVDF form by the presence of vibrations found at 763, 875 and 978 cm^{-1}. In the infrared spectra of PVDF films containing $BaTiO_3$ particles and with different concentrations, a higher intensity of the band located at 837 cm^{-1} in PVDF-70% is observed, compared to the band located at 839 cm^{-1} in PVDF-30%, and this attests the presence of $BaTiO_3$ particles at different concentrations.

Finally, in the PVDF solution with solvent, initially used to obtain the film, polymer-solvent interactions occur, that involves strong dipolar interactions between the dipole C = O and CH_2 - CF_2 and can induce the presence of weak hydrogen bonds between C = O and H - C. These interactions also play an important role in PVDF crystallization [58].

In this sense, the dipolar interaction and hydrogen bonding at the interface between the crystal nucleus and the solvent molecules will lead to a total planar configuration of CH_2 - CF_2 dipoles, when nucleation occurs at room temperature [59, 60].

If there is a relatively large external energy, such as thermal energy, and this is supplied during the crystallization process, the forces that are at the origin of the interactions in the polymer chains become weak to cause the PVDF molecules to crystallize in the trans-gauche α-PVDF conformation, which is thermodynamically more stable. When $BaTiO_3$ nanoparticles are added to the solution, stronger O-H and F-C hydrogen bonds are probably formed due to the high polarity of the hydroxyl groups; the ceramic nanoparticles thus act as nucleating agents for PVDF. The strong O-H and F-C hydrogen interaction at $BaTiO_3$ nanoparticle/PVDF interfaces, together with the dipolar interactions between PVDF and the solvent, tend to produce locally oriented CH_2-CF_2 dipoles in the characteristic configuration for the β crystallization mode. The nucleation of the β phase is proportional to the increase in the ceramic concentration of $BaTiO_3$ nanoparticles and is corresponding to the decrease in the "trans-gauche" configuration characteristic of non-electroactive α-PVDF crystallization.

This hypothesis is supported by the absorption band between 3100 and 3700 cm^{-1} attributed to the hydrogen bond νO – H [61], this band not being characteristic for the pure polymer.

3.3. Dielectric tests

The dielectric tests presumed the broadband analysis vs. frequency of both BT-PDMS and BT-PVDF composites in freestanding state, as regards dielectric permittivity and dielectric loss, Figures 6-8, followed by the evolution vs. frequency of the impedance of the films mainly deposited on specific substrates, as ITO 0.05 mm thick and PET 0.1 mm thick, Figures 9-12 respectively. Due to the fact that composites type PVDF-BT are more widely described in literature, more attention in this paper regarding the dielectric and piezoelectric features is allocated to PDMS-BT composites.

The lower values for dielectric permittivity and tgδ, comparing to the materials described in the literature - made exclusively from BT particles, are explained by the composite structure, which contains electrically active particles, but dispersed in a relatively large quantity of polymers. For PDMS composites, the dielectric permittivity decreases with applied frequency, and increases with the quantity of BT in composites, e.g. from 3.73 for 30%BT-70%PDMS to 4.52 for 70%BT-30%PDMS at 10Hz. The evolution with frequency for tgδ is as expected, influenced by interfacial polarization at lower frequencies, and the dipolar one at higher frequencies. At lower frequencies, the interfacial polarization is more active at larger quantities of BT particles, e.g. tgδ varies from 0.065 for 30%BT-70%PDMS to 0.014 for 70%BT-30%PDMS at 10Hz. An interesting effect is observed at about 80 kHz, respectively a pic of the tgδ characteristic, to be correlated to the activity and architecture of BT particles, which induce an additional ionic-dipolar conjugated polarization, e.g. a displacement due to the balance between the resonance and anti-resonance frequency. Such phenomena explain the use of composites with ferrites or piezoelectric powders as resonators/filters, and BT-PDMS composites should be further investigated for tailored applications in radiofrequency electronic field. There can be noticed a clear correlation of the

frequency domain from where this phenomenon occurs, at both permittivity and tgδ characteristics (in the case of permittivity, a slow increase is noticed).

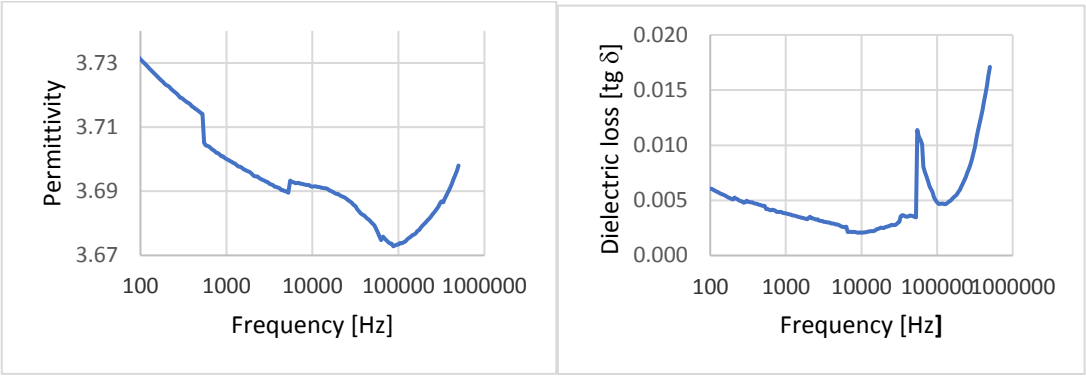

Figure 6. Dielectric behavior of 30%BT-70%PDMS 320µm, freestanding

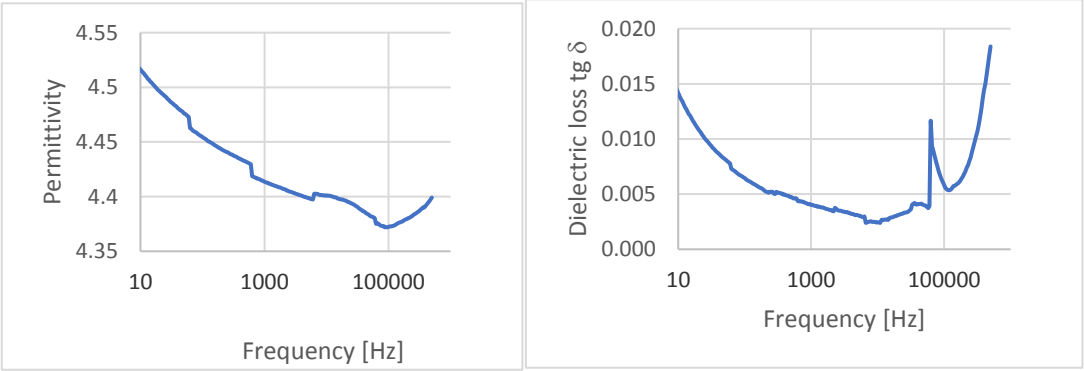

Figure 7. Dielectric behavior of 70%BT-30%PVDF 200µm, freestanding

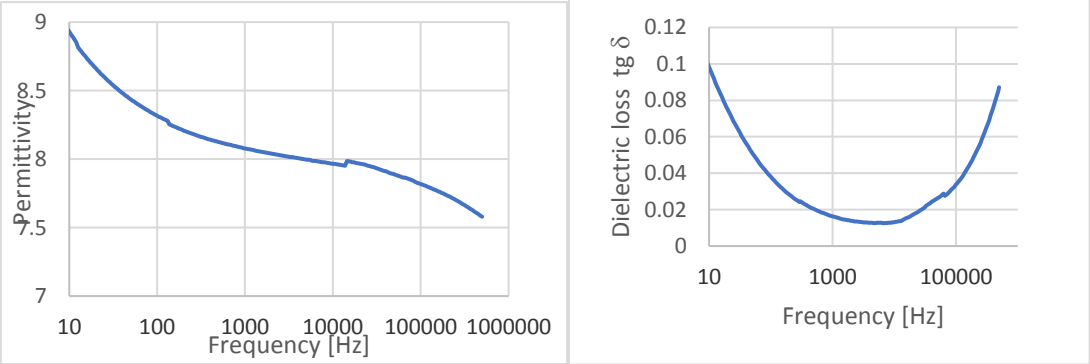

Figure 8. Dielectric behavior of 30%BT-70%PVDF 110µm, freestanding

As regards the PVDF composites, the evolution of the dielectric characteristics are similar, i.e. the dielectric permittivity decreases with applied frequency and the tgδ characteristic presents two increased zones for the two polarization types, as presented above. Here we can also notice a very limited domain of frequency around 50kHz where the effect of piezoelectric activity alters the characteristics, but the effect is very weak comparing to the PDMS composites.

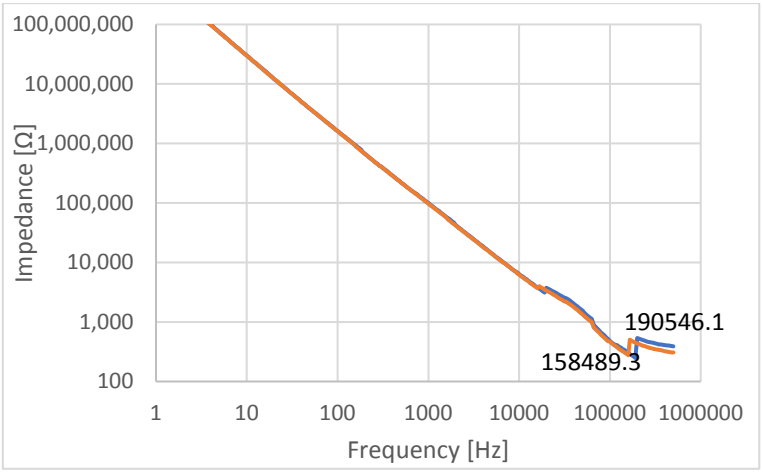

Figure 9. Impedance of 30%BT-70%PDMS on ITO: 270µm (blue); 110µm (red)

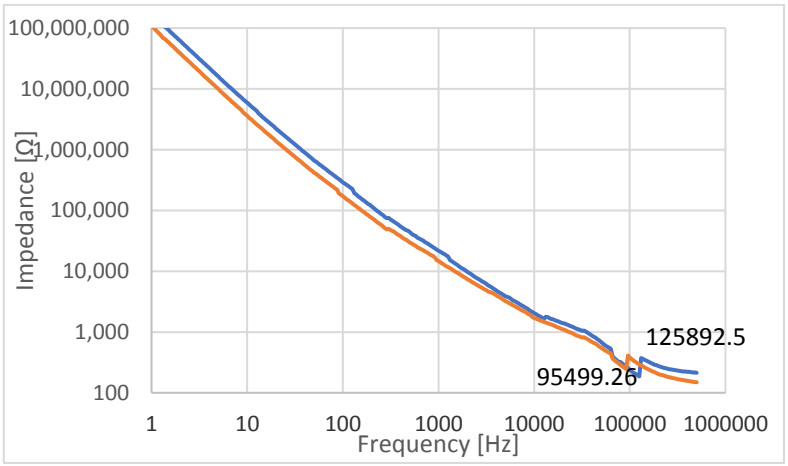

Figure 10. Impedance of 70%BT-30%PDMS on PET: 230µm (blue); 130µm (red)

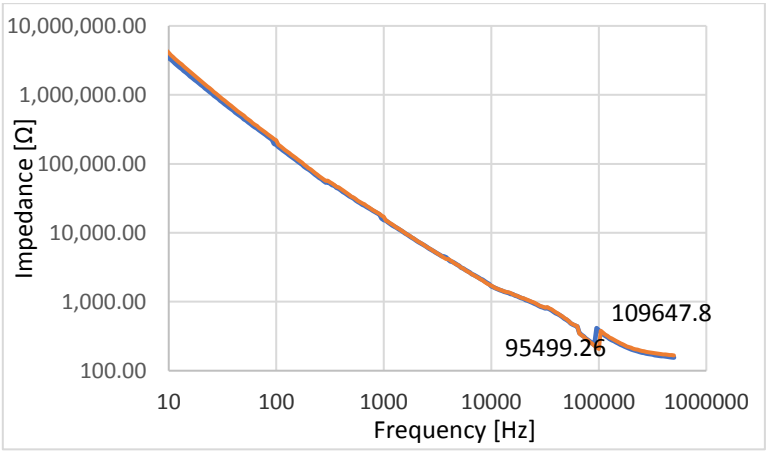

Figure 11. Impedance of 30%BT-70%PVDF on ITO: 220µm (blue); 120µm (red)

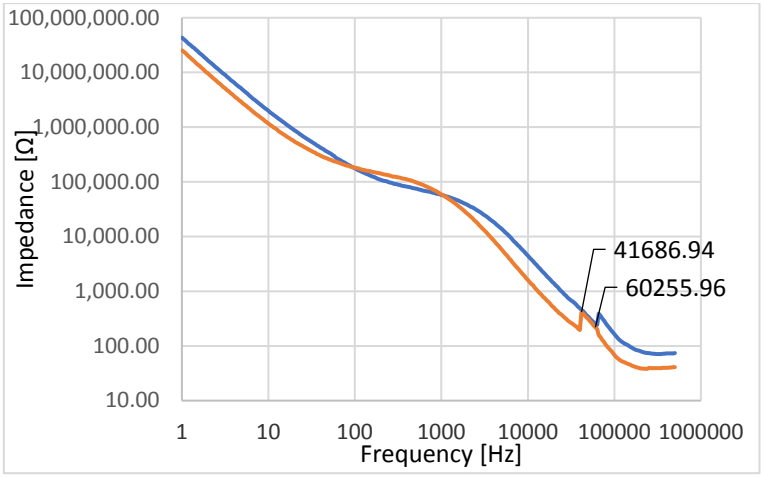

Figure 12. Impedance of 70%BT-30%PVDF on PET: 220µm (blue); 120µm (red)

As long as the most applications of piezoelectric composites fall in the domain of wearable or tactile electronics, the impedance of such preliminary devices is analyzed, (Figures 9-12) not in the freestanding state, but as deposited on tailored support in relation with the potential applications, e.g. ITO/glass 0.05mm thick and PET 0.1mm thick. The displacement related to the resonance and anti-resonance frequency is herewith also visible, the frequencies related to the picks being presented on the figures. The higher values of the impedance at lower frequencies are determined by the substrate, which is in the class of electrical insulators.

The impedance of 30%BT-70%PDMS on ITO, Figure 10 seems to be insensible to the sample thickness, a visible difference being noticed only after the 100 kHz domain, where the resonance/anti-resonance frequency occurs. The same observation is valid also for the sample 30%BT-70%PVDF on ITO (Figure 11) but in this case the resonance/antiresonance frequency is slightly lower than 100 kHz domain. In these cases, we may say that the samples thickness has no relevant influence on impedance, but the polymer matrix minor influence is yet visible.

Clear influence of sample thickness upon impedance is noticed for higher content of BT, e.g. for the sample 70%BT-30%PDMS on PET (Figure 10) where the resonance/antiresonance frequency is also visible by the same frequency domain of 100k Hz. Comparing Figures 9 and 10, one side, and 11 and 12, on the other side, we may say that the substrate has no major influence upon the resonance/ antiresonance frequency for thicker samples of over 200µm.

Particular behavior presents the sample 70%BT-30%PVDF on PET, Figure 12, where the difference of impedance vs. sample thickness is obvious, and the characteristic shape being amplified also by the feature of PVDF polymer matrix. Here, after 1k Hz domain, the characteristics are clearly divergent, only by comparing with Figure 10, where the PDMS matrix was used.

After measuring the samples, it was found that in the case of the 30% BT-70% PDMS samples, the electrical impedance is about 30% lower than in the case of the 70% BT-30% PDMS samples after 1 kHz domain. Contrarily, in the case of the 30% BT-70% PVDF and 70% BT-30% PVDF samples, the electrical impedance keeps practically the values in all frequency domain, excepting that there is a clear difference in resonance/antiresonance frequency value, the values being significantly lower in the case with more content of BT, observations in line with [62 - 64].

Finally, we may conclude that the thickness of the samples has a major influence in the displacement of the resonance/anti-resonance frequency, in the sense that it leads to the displacement to the left in the frequency domain.

3.4. Piezoelectric characteristics

The hysteresis curves were raised at the frequency of 0.1 Hz, with an electrical voltage of about 80% of the respective breakdown voltage values. The study was performed at different voltages for different BT content and substrates, in order to have a clear picture upon the occurring phenomena.

From the hysteresis curves, it is observed that in the case of both composites' types of $BaTiO_3$-Polydimethylsiloxane and $BaTiO_3$-Polyvinylidene difluoride clear hysteresis curves are obtained, quasi-homogeneous, but unsaturated at the used voltages (Figures 13-18).

A first analysis was made vs. material thickness, and in all figures, it was noticed that the increase of the material thickness, i.e. a larger quantity of PD powder, leads to superior values of energy and higher polarization. This is obvious when comparing the pair of samples exposed to the same voltage, e.g. in Figures 13, 14, 17 and 18, the substrate having no relevant influence. A small difference occurs when comparing samples in freestanding state with the ones on support, e.g. Figures 15 with 16 and 18. Here, the same polarization seems to need a superior voltage for the samples in freestanding state, but in this case the energy is substantially higher, e.g. 3.5 μJ/cm^2 for the sample 30%BT-70%PDMS on ITO, comparing to 68 μJ/cm^2 for similar sample freestanding. When taking into account the samples with higher BT content on PET, e.g. 70%BT-30%PDMS even if with low thicknesses, the substrate permits a major increase of the applied voltage, and the characteristics can be turned towards saturation.

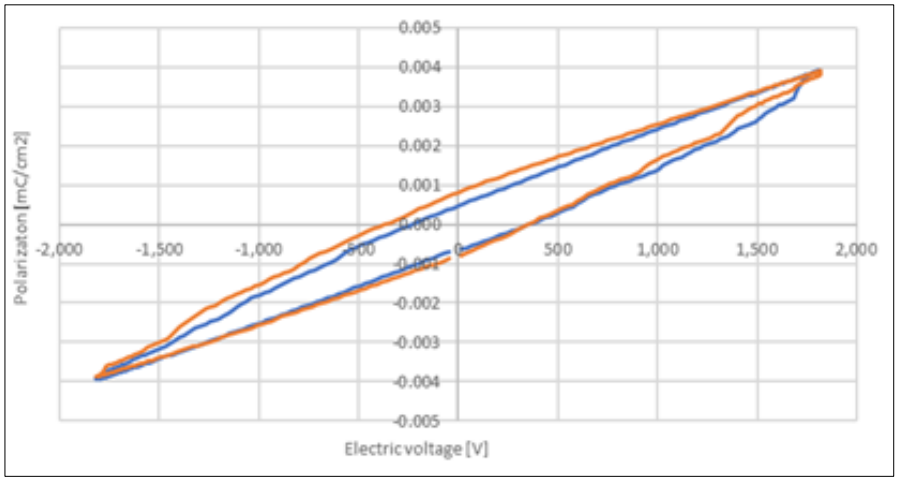

30%BT-70%PDMS – 270 μm on PET (red)	30%BT-70%PDMS – 110 μm on PET (blue)
Area[mm^2]: 800	Area[mm^2]: 800
Electrical intensity [nA]: 100	Electric intensity [μA]: 1
Frequency [Hz]: 0.1	Frequency [Hz]: 0.1
Electric voltage [V]: 2500	Electric voltage [V]: 2500
Vc+ [V]: 305.589	Vc+ [V]: 307.416
Pr+ [μC/cm^2]: 0.000437322	Pr+ [μC/cm^2]: 0.000335157
P_{max} [μC/cm^2]: 0.00361861	P_{max} [μC/cm^2]: 0.00289493
W_{loss} [μJ/cm^2]: 3.42454	W_{loss} [μJ/cm^2]: 2.81265

Figure 13. Hysteresis characteristics for 30%BT-70%PDMS composites on PET support

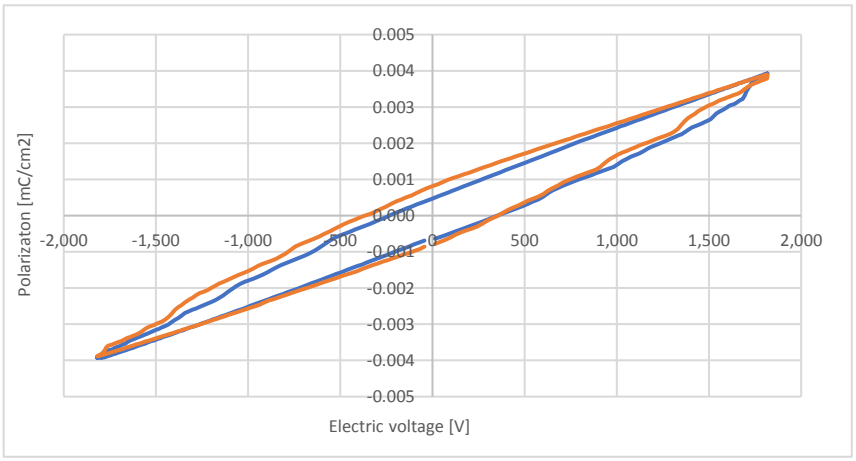

30%BT-70%PDMS - 310µm on ITO (red) Area [mm^2] 507 Electric intensity [µA]: 1 Frequency [Hz]: 0.1 Electric voltage [V]: 1800 Vc+ [V]: 343.157 Pr+ [µC/cm^2]: 0.000810109 Pmax [µC/cm^2]: 0.00388204 W_{loss} [µJ/cm^2]: 3.58983	30%BT-70%PDMS - 100µm on ITO (blue) Area [mm^2] 558 Electric intensity [nA]: 100 Frequency [Hz]: 0.1 Electric voltage [V]: 1800 Vc+ [V]: 338.653 Pr+ [µC/cm^2]: 0.000472076 Pmax [µC/cm^2]: 0.00392282 W_{loss} [µJ/cm^2]: 2.91856

Figure 14. Hysteresis characteristics for 30%BT-70%PDMS composites on ITO support

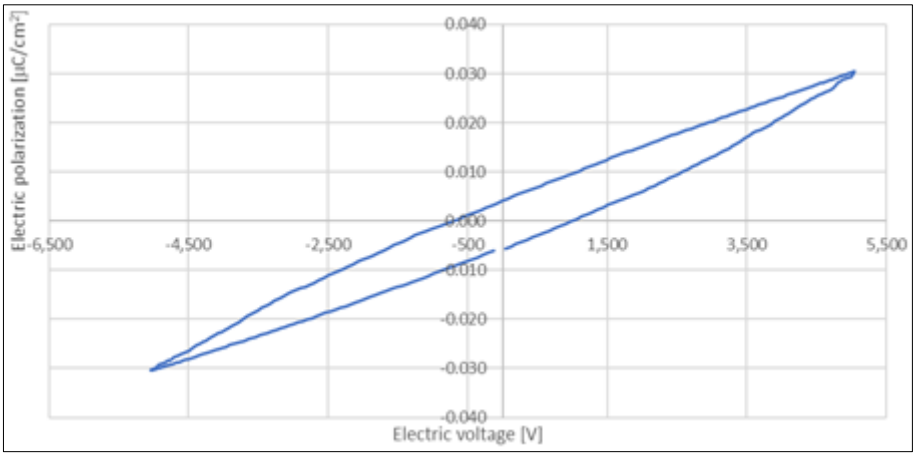

30%BT-70% PDMS – 320 µm freestanding
Area [mm^2]: 158.71
Electric intensity [nA]: 100nA
Frequency [Hz]: 0.1
Electric voltage [V]: 5000
Vc+ [V]: 952.029
Pr+ [µC/cm^2]: 0.0041009
P_{max} [µC/cm^2]: 0.0304191
W_{loss} [µJ/cm^2]: 68.2683

Figure 15. Hysteresis characteristics for 30%BT-70%PDMS composite, freestanding

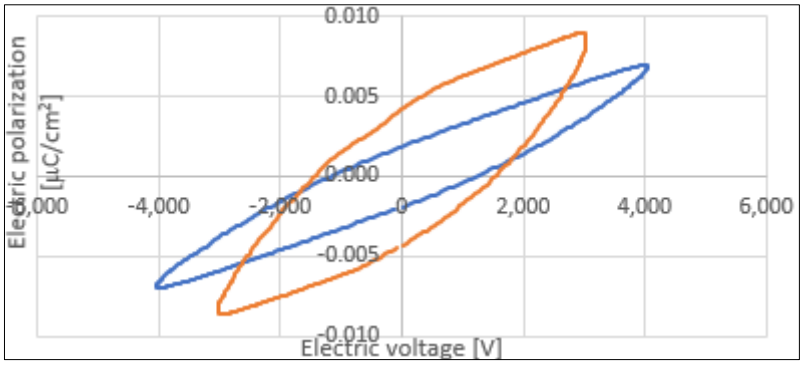

70%BT-30% PDMS – 200 μm on PET (red) Area [mm^2]: 646 Electric intensity [nA]: 100nA Frequency [Hz]: 0.1 Electric voltage [V]: 4000 Vc+ [V]: 1515.31 Pr+ [μC/cm^2]: 0.00420067 P_{max} [μC/cm^2]: 0.00852436 W_{loss} [μJ/cm^2]: 37.3918	70%BT-30%PDMS – 130 μm on PET (blue) Area [mm^2]: 608.45 Electric intensity [nA]: 100nA Frequency [Hz]: 0.1 Electric voltage [V]: 3000 Vc+ [V]: 1197.48 Pr+ [μC/cm^2]: 0.00186451 P_{max} [μC/cm^2]: 0.0068621 W_{loss} [μJ/cm^2]: 22.4647

Figure 16. Hysteresis characteristics for 70%BT-30%PDMS composites on PET support

Clear piezoelectric effects are also observed for the BT-PVDF type composites, but here the thickness and substrate seem not to influence in a significant way the polarization values, and the energy values are also relatively close if comparing with freestanding state (at the same applied voltage). No remarkable piezoelectric effects are also observed when comparing the sample 70%BT-30%PVDF with the sample 30%BT-30%PVDF, the polarization and energy being very close as values. In all, we can appreciate that superior piezoelectric features are offered by the composites of BT with PDMS, comparing to the composites with PVDF, which means that the composites of BT with PDMS were worth to study, leading to more versatile variants of characteristics and with superior values.

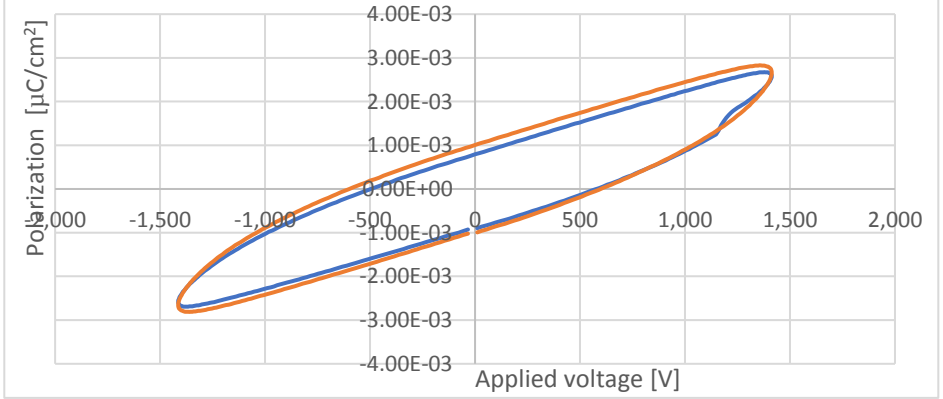

30%BT-70%PVDF - 110 μm on PET (blue) Area [mm^2]: 599.02 Electric intensity [nA]: 100nA Frequency [Hz]: 0.1 Electric voltage [V]: 1400 Vc+ [V]: 568.268 Pr+ [μC/cm^2]: 0.000792963 P_{max} [μC/cm^2]: 0.00258135 W_{loss} [μJ/cm^2]: 3.89556	30%BT-70%PVDF 220 μm freestanding (red) Area [mm^2]: 590.86 Electric intensity [nA]: 100nA Frequency [Hz]: 0.1 Electric voltage [V]: 1400 Vc+ [V]: 587.547 Pr+ [μC/cm^2]: 0.00100454 Pmax [μC/cm^2]: 0.00266538 Wloss [μJ/cm^2]: 4.63826

Figure 17. Hysteresis characteristics for 30%BT-70%PVDF composites on PET support

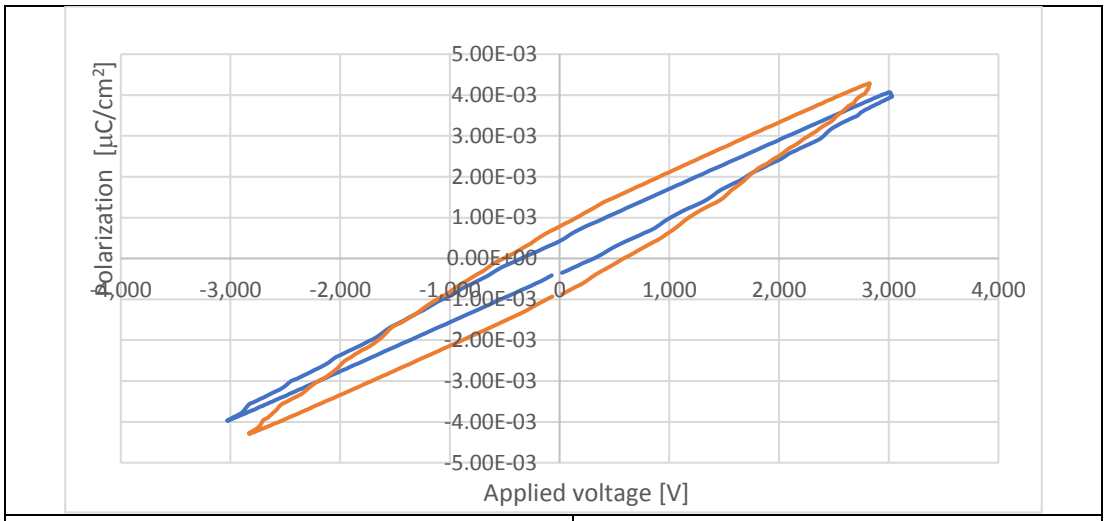

70%BT-30%PVDF - 120μm on PET (blue) Area [mm²]: 665.3 Electric intensity [nA]: 100nA Frequency [Hz]: 0.1 Electric voltage [V]: 2800 Vc+ [V]: 287.968 Pr+ [μC/cm²]: 0.000422156 P_{max} [μC/cm²]: 0.00397102 W_{loss} [μJ/cm²]: 3.24087	70%BT-30%PVDF - 220μm freestanding (red) Area [mm²]: 675.46 Electric intensity [nA]: 1uA Frequency [Hz]: 0,1 Electric voltage [V]: 3000 Vc+ [V]: 562.019 Pr+ [μC/cm²]: 0.000785376 P_{max} [μC/cm²]: 0.0042818 W_{loss} [μJ/cm²]: 6.11345

Figure 18. Hysteresis characteristics for 70%BT-30%PVDF composites on PET support

3.5. Development and test of flexible piezoelectric structures

The experimental model for the vibration motion is simulated as a function of different displacement of the piezoelectric film, corresponding to the resonant frequency, and the variation of electrical voltage corresponding to the length and thickness of the film. For the development and integration of the signal processing circuits and the demonstration of the functionality of the energy harvesting features of the flexible piezoelectric structures, a special test stand was developed, as in Figure 19, to produce tailored vibrations to activate the devices – here with functionality as piezoelectric sensors. To realize sensorial features, the structures are covered on both sides with self-adhesive copper strips in order to collect the electrical charges obtained by piezoelectric phenomena.

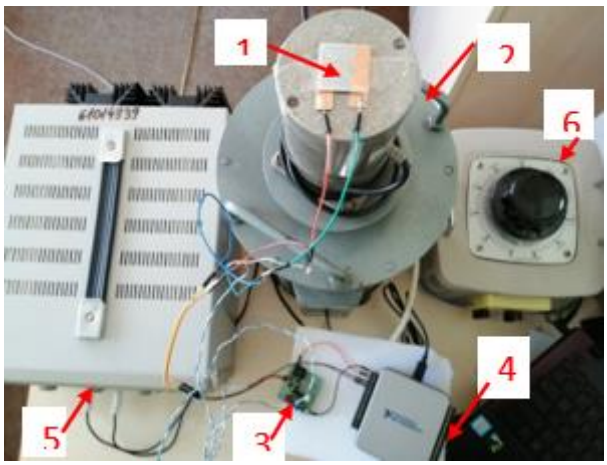

Figure 19. The test stand used for the production and acquisition of the signal,
where: 1 – device/sensor; 2 – vibration creation equipment; 3 – capacitor charging circuit; 4 – NI USB acquisition board – 6001; 5 – direct current source (constant voltage 24V); 6 – autotransformer (alternating voltage supply) – for vibration increase/decrease regime

To generate the vibrations, a specialized equipment (2) with two windings was used (composed of a fixed part and a mobile part, the mobile part being connected to the fixed one by means of an elastic mechanical suspension), supplied with a constant voltage of 24V dc from the direct voltage source (5), and also with alternating voltage from the autotransformer (6). The vibration force is proportional with the currents absorbed by the two windings according to equation 1:

$$F_{din}=kI_{cc}I_{ca} \quad (1)$$

The vibration amplitude was proportional to F_{din}.

Firstly, it has been studied how the variations in the resonant frequencies of the structure, which affect the piezoelectric electric energy, are affected by the length (which varies from 1 cm to 10 cm), width (up to 1 cm) and thickness (up to 0.6 mm) of a cantilever made with the composite type 70%BT-30%PDMS, deposited on a PET support of 0.1 mm thickness.

The results of the different electromechanical simulations are showing: a) that the resonant frequency dramatically decreases with the length of the model, when the width and thickness are constant, and b) that the beam width and respectively thickness have a significant influence on the resonance frequency, with a saturation tendency. Basically, it is noticed that all geometric elements can influence the resonance frequency, which is maximum at a minimum length, at larger thicknesses and larger widths of the experimental model. But if we target the biomedical applications, e.g. for portable electronics, with resonance frequencies up to 10Hz, the ideal dimensions are about 10 cm long, 0.5 cm wide and 0.15-0.2 mm thick.

Similarly, it is shown that the output voltage depends on the geometric dimensions, showing the variation of the output voltage with the model length (non-linear) and thickness. The maximum output voltage is obtained when the length is maximum, and thickness is lower, so in line with the optimal dimensions for biomedical applications. The higher voltage is explained by a larger quantity of BT in the model when the force is applied perpendicular to the surface, so achieved e.g. at higher length. The relatively low values of voltage, of under 1V, are explained by the composite structure, which contains electrically active particles, but dispersed in a relatively large quantity of polymers.

The experimental model can be further customized in a versatile way depending on: the parameters of the piezoelectric material and the dimensional availability, to program, by adjusting the architecture of the piezo structure, the desired resonance frequency, and then to calculate the output voltage, depending on which the AC circuit and the AC/DC converter are designed.

A brief demonstration of the behavior of composites as energy harvester devices is presented below, also for the composite of PDMS with 70% $BaTiO_3$. The intelligent signal processing was made by use of a virtual instrument (VI) developed under LabVIEW graphical programming environment [65], briefly presented in Figures 20 and 21, in relation with a specialized acquisition board.

In structure 1 from Figure 20, a CASE structure was used, in which the first time it is checked if it is the first run of the program. If it is the first run, the case is TRUE and a "task" is opened using the "DAQmx Create Task" tool. If it is not on the first run, it will pass to FALSE and the session opened the first time will be processed.

In structure 2, a CASE structure was used, in the case of TRUE, the acquisition board to be used is selected (if there are several), and also the analog channel on which the signal acquisition will be made will be selected. The FALSE case occurs after the first run, in which case the board and acquisition channel have been set.

In structure 3, another CASE structure was used to be able to modify the size to be applied to the input of the purchase board. Since the piezoelectric module at the output provides a voltage, "Voltage" was selected, then the RSE module will be configured. Another way the board works is differential but in this configuration the signal is not differential. If the CASE structure is in the "FALSE" configuration, the configuration tool will disappear from the diagram, which means that no acquisition board has been detected.

In area 4 of Figure 20, the configuration parameters for the analog input are highlighted. Being an RSE type input, the "floating" type input voltage limits were set with "-10 V" and "10 V" values.

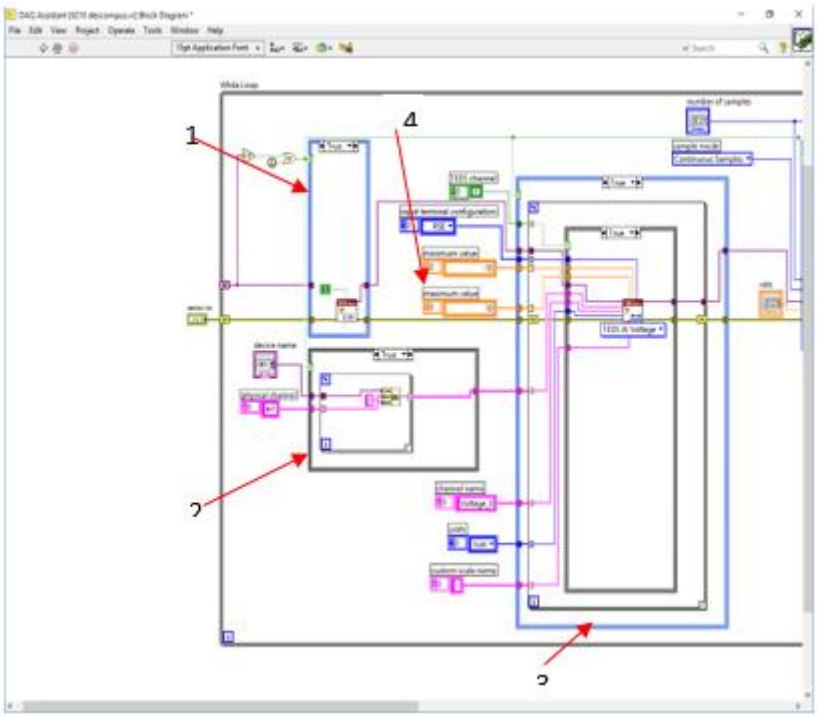

Figure 20. VI - part of the acquisition board configuration/programming

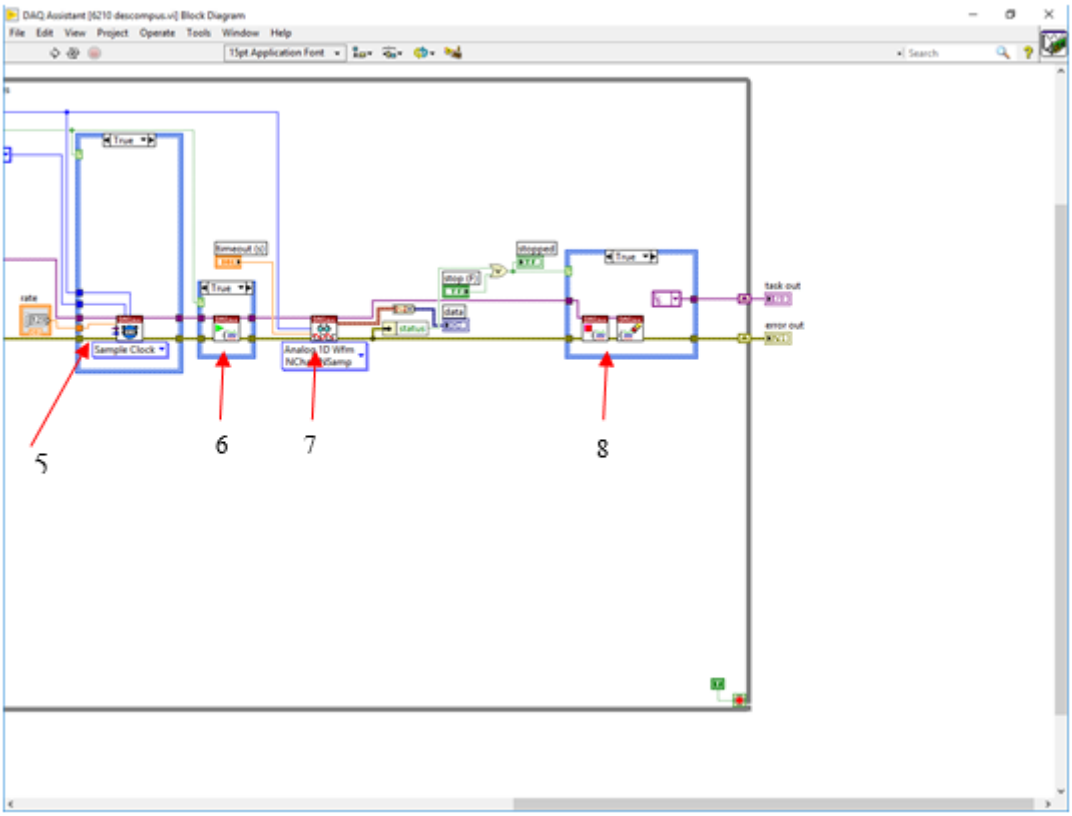

Figure 21. VI - part of the acquisition procedure interface

In Figure 21, area 5 shows the diagram for configuring the number of samples acquired in a unit of time. The sampling rate is also set. After this, the next CASE loop is executed, denoted by 6. At this stage, the program opens a "task" through which the acquisition of the signal is prepared.

Also, if in addition to signal acquisition, the generation of signals of various shapes and frequencies is also desired, this "task" will take care of this.

In area 7 of Figure 21, the instantaneous values of the signal are acquired as a function of the sampling frequency. The results will be presented as a 1D vector. Then the data in the 1D dimension vector is converted to "dynamic data type" (DDT).

In area 8, the CASE structure deals with closing the work session when the "STOP" button is pressed in the main loop or when an error occurs in the execution of the program and a "STOP" condition is activated. The demonstration device is presented in Figure 22, based on a demonstration board which converts the energy generated by the piezo-sensor towards lighting a LED.

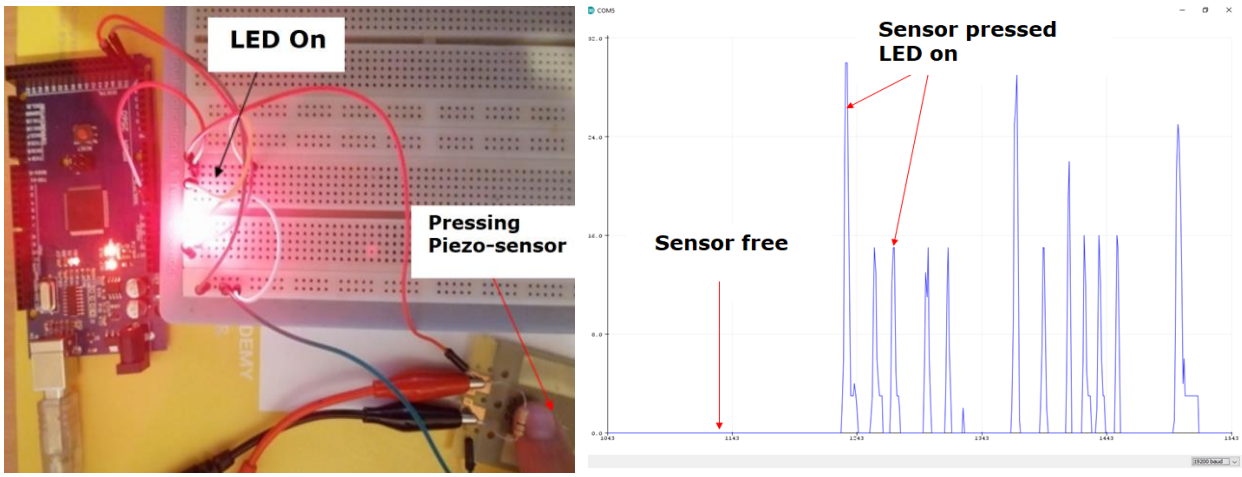

Figure 22. Demonstration device with LED, and signals evolution vs. LED activity

An example of demonstration signals in relation with the LED activity is presented in Figure 22, which shows the evolution of the output voltage value for a multilayer piezoelectric sensor, when the sensor is not pressed and when the sensor is pressed with different forces (e.g. for the demonstration, with a finger). Depending on the pressing force, the voltage value at the sensor output varies, the higher the force, the higher the voltage and the stronger the light intensity of LED. Also, the longer the pressing time, the wider the pulse of the output signal will be, but with a decreasing value, due to the oscillation damping, i.e. the last signal in Figure 22.

In principle, the experiment basically demonstrates the functionality of the piezoelectric thin film composites with $BaTiO_3$, which can be successfully used both as piezo-sensors for microelectronics, or for energy harvesting purposes, ideally for applications in biomedical wearable electronics.

4. Conclusions

The piezocomposites from PVDF with BT are largely presented in literature, but the composites from PDMS with BT consist a very new scientific preoccupation. The innovation presented in the paper lies in the new simple route of preparation of the two composites with PDMS and respectively PVDF matrix, with tailored deposition on specific substrates for microelectronic use (e.g. indium-tin-oxide ITO/glass, Si/Pt, polyethylene terephthalate PET), along with an extensive comparation of their dielectric and piezo-electric features, as a consistent comparison of the influence of polymer matrix upon the piezoelectric features, and a demonstration of direct use for microelectronic applications of the composites of BT with PDMS.

Two types of composite films were made from thermoplastic polymer matrix: polyvinylidene fluoride (PVDF) and respectively polydimethylsiloxane (PDMS), doped with tetragonal $BaTiO_3$ (BT) particles of irregular shape (< 2 μm dimension), with 2 concentrations for each composite type (30%

and 70% $BaTiO_3$). The samples were manufactured on different support (ITO/glass, Si/Pt and PET– the last one being used for extracting freestanding films too) were manufactured, with different thicknesses, to test their features in order to potentially become successful candidates for microelectronic applications with, or without support.

An extensive characterization of composites via Fourier transform infrared spectra was performed, to account for the liaisons of the BT particles with polymer matrix.

The dielectric tests presumed the broadband analysis vs. frequency of both BT-PDMS and BT-PVDF composites, as regards dielectric permittivity and dielectric loss. For both composite types, the dielectric permittivity decreases with applied frequency, and increases with the quantity of BT in composites. The evolution with frequency for tgδ is influenced by interfacial polarization at lower frequencies, and the dipolar one at higher frequencies. An interesting effect is observed around 100 kHz domain, determined by the activity and architecture of BT particles mainly for the BT-PDMS composites, which induce an additional ionic-dipolar conjugated polarization, as a displacement due to the balance between the resonance and anti-resonance frequency. Such phenomena explain the potential use of such composites as resonators/filters, and BT-PDMS composites should be further investigated for tailored applications in radiofrequency electronic field.

The impedance of 30%BT-PVDF or PDMS composites seems to be insensible to the sample thickness, but the polymer matrix minor influence is yet visible. Clear influence of sample thickness upon impedance is noticed for higher content of BT. We may also conclude that the thickness of the samples has a major influence in the displacement of the resonance/anti-resonance frequency, in the sense that it leads to the displacement to the left in the frequency domain

The hysteresis curves were raised at the frequency of 0.1 Hz, with an electrical voltage of about 80% of the respective breakdown voltage values. The study was performed at different voltages for different BT content and substrates, in order to have a clear picture upon the occurring phenomena. It was noticed that the increase of the material thickness, i.e. a larger quantity of PD powder, leads to superior values of energy and higher polarization, and also a small difference occurs when comparing samples in freestanding state with the ones on different support. No remarkable piezoelectric effects were observed when comparing the sample 70%BT-30%PVDF with the sample 30%BT-30%PVDF, the polarization and energy being very close as values. In all, we can appreciate that superior piezoelectric features are offered by the composites of BT with PDMS, comparing to the composites with PVDF, which means that the composites of BT with PDMS were worth to study, leading to more versatile variants of characteristics and with superior values.

The experimental model for the vibration motion is simulated as a function of different displacement of the piezoelectric film, corresponding to the resonant frequency, and the variation of electrical voltage corresponding to the length and thickness of the film, that finally emphasized that the resonant frequency dramatically decreases with the length of the model, when the width and thickness are constant, and also that the beam width and respectively thickness, have a significant influence on the resonance frequency, with a saturation tendency.

A brief demonstration of the behavior of composite of PDMS with 70% $BaTiO_3$ as energy harvester devices was presented. The intelligent signal processing was made by use of a virtual instrument developed under LabVIEW graphical programming environment. The experiment basically demonstrated the functionality of the piezoelectric thin film composites of PDMS with $BaTiO_3$, which can be successfully used both as piezo-sensors for microelectronics, or for energy harvesting purposes, ideally for applications in biomedical wearable electronics or tactile electronics.

Acknowledgments: This work was supported by a publication grant of Technical Univ. Iasi, and it was based on a joint experimental research, partially financed by a grant under COFUND-ERANET MANUNET III (HarvEnPiez). Special thanks go to Dr. Špela Kunej and the related research team from the "Jožef Stefan" Institute, Ljubljana, Slovenia, for the support in samples preparation.

References

1. WANG, A.C., WU, C., PISIGNANO, D., WANG, Z.L., PERSANO, L., Polymer nanogenerators: opportunities and challenges for large-scale applications, *J. Appl. Polym. Sci.*, 134, 2017, 45674. https://doi.org/10.1002/app.45674
2. PANDA, P.K., SAHOO, B., PZT to lead free piezo ceramics: a review, *Ferroelectrics*, 474, 2015, 128-143. https://doi.org/10.1080/00150193.2015.997146
3. KANG, H.B., HAN, C.S., PYUN, J.C., RYU, W.H., KANG, C.Y., CHO, Y.S., $(Na,K)NbO_3$ nanoparticle-embedded piezoelectric nanofiber composites for flexible nanogenerators, *Compos. Sci. Technol.*, 111, 2015, 1-8. https://doi.org/10.1016/j.compscitech.2015.02.015
4. CHERNOZEM, R.V., SURMENEVA, M.A., SURMENEV, R.A., Hybrid biodegradable scaffolds of piezoelectric polyhydroxybutyrate and conductive polyaniline: piezocharge constants and electric potential study, *Mater. Lett.*, 220, 2018, 257-260. https://doi.org/10.1016/j.matlet.2018.03.022
5. CHEN, X., TIAN, H., LI, X., SHAO, J., DING, Y., AN, N., ZHOUA, Y., A high performance P(VDF-TrFE) nanogenerator with self-connected and vertically integrated fibers by patterned EHD pulling, *Nanoscale*, 7, 2015, 11536-11544. https://doi.org/10
6. SHI, J., YONG, S., BEEBY, S., An easy to assemble ferroelectret for human body energy harvesting, *Smart Mater. Struct.*, 27, 2018, 084005. https://doi.org/10.1088/1361-665X/aabdbc
7. NARITA, F., FOX, M., A review on piezoelectric, magnetostrictive, and magnetoelectric materials and device technologies for energy harvesting applications, *Adv. Eng. Mater.*, 20, 2018, 1700743. https://doi.org/10.1002/adem.201700743.
8. MARTINS, P., LOPES, A., LANCEROS-MENDEZ, S., Electroactive phases of poly (vinylidene fluoride): determination, processing and applications, *Prog. Polym. Sci.*, 39, 2014, 683-706. https://doi.org/10.1016/j.progpolymsci.2013.07.006.
9.VINSON, J.H., JUNGNICKEL, B.J., Structure and stress dependence of pyroelectricity in poly (vinylidene fluoride), *Ferroelectrics*, 216, 1998, 63-81. https://doi.org/10.1080/00150199808018228
10. ZHAO, J., YOU, Z., A shoe-embedded piezoelectric energy harvester for wearable sensors, *Sensors*, 14, 2014, 12497-12510. https://doi.org/10.3390/s140712497
11. KIM, Y.W., LEE, H.B., MO YEON, S., PARK, J., LEE, H.J., YOON, J., PARK, S.H., Enhanced piezoelectricity in a robust and harmonious multilayer assembly of electrospun nanofiber mats and microbead-based electrodes, *ACS Appl. Mater. Interfaces*, 10, 2018, 5723-5730. https://doi.org/10.1021/acsami.7b18259.
12. JEONG, C.K., BAEK, C., KINGON, A.I., PARK, K.I., KIM, S.H., Lead-free perovskite nanowire-employed piezopolymer for highly efficient flexible nanocomposite energy harvester, *Small*, 14, 2018, 1704022. https://doi.org/10.1002/smll.201704022
13. YANG, G., YUE, Z., ZHAO, J., WEN, H., WANG, X., LI, L., Dielectric behaviour of $BaTiO_3$-based ceramic multilayer capacitors under high dc bias field, *J. Phys. D Appl. Phys.*, 39(16), 2006, 3702-3707.
14. ZHANG, X., MA, Y., ZHAO, C., YANG, W., High dielectric constant and low dielectric loss hybrid nanocomposites fabricated with ferroelectric polymer matrix and $BaTiO_3$ nanofibers modified with perfluoroalkylsilane, *Appl. Surf. Sci.*, 305, 2014, 531-538.
15. HU, P., SUN, W., FAN, M., QIAN, J., JIANG, J., DAN, Z., LIN, Y., NAN, C.-W., LI, M., SHEN, Y., Large energy density at high-temperature and excellent thermal stability in polyimide nanocomposite contained with small loading of $BaTiO_3$ nanofibers, *Appl. Surf. Sci.*, 458, 2018, 743-750.
16. TAO, J., CAO, S.-A., FENG, R., DENG, Y., High dielectric thin films based on barium titanate and cellulose nanofibrils, *RSC Adv.*, 10(10), 2020, 5758-5765.
17. MAYEEN, A., KALA, M.S., SUNIJA, S., ROUXEL, D., BHOWMIK, R.N., THOMAS, S., KALARIKKAL, N., Flexible dopamine-functionalized $BaTiO_3$/$BaTiZrO_3$/$BaZrO_3$-PVDF ferroelectric nanofibers for electrical energy storage, *J. Alloys Compd.*, 837, 2020.

18. KAKIMOTO, K.-I., FUKATA, K., OGAWA, H., Fabrication of fibrous $BaTiO_3$-reinforced PVDF composite sheet for transducer application, *Sens. Actuators A-Phys.*, 200, 2013, 21-25.
19.GAO, J., XUE, D., LIU, W., ZHOU, C., REN, X., Recent progress on $BaTiO_3$-based piezoelectric ceramics for actuator applications, *Actuators*, 6(3), 2017, 24.
20. ACOSTA, M., NOVAK, N., ROJAS, V., PATEL, S., VAISH, R., KORUZA, J., ROSSETTI, G.A., R¨ODEL, J., $BaTiO_3$-based piezoelectrics: fundamentals, current status, and perspectives, *Appl. Phys. Rev.*, 4(4), 2017, 041305.
21.SEBASTIAN, T., LUSIOLA, T., CLEMENS, F., Ferroelectric hybrid fibers to develop flexible sensors for shape sensing of smart textiles and soft condensed matter bodies, *Smart Mater. Struct.*, 26(4) 2017.
22. SEBASTIAN, T., MICHALEK, A., HEDAYATI, M., LUSIOLA, T., CLEMENS, F., Enhancing dielectric properties of barium titanate macrofibers, *J. Eur. Ceram. Soc.*, 39(13) 2019, 3716-3721.
23.WANG, L., HE, Y., HU, J., QI, Q., ZHANG, T., DC humidity sensing properties of $BaTiO_3$ nanofiber sensors with different electrode materials, *Sens. Actuators B Chem.*, 153(2), 2011, 460-464.
24.VEERALINGAM, S., RAVINDRANATH, A.N.K., BADHULIKA, S., Low cost, flexible, perovskite $BaTiO_3$ nanofibers-based p–n homojunction for multifunctional sensing of physical and chemical stimuli, *Adv. Mater. Interfaces*, 2020.
25.WANG, F., MAI, Y.-W., WANG, D., DING, R., SHI, W., High quality barium titanate nanofibers for flexible piezoelectric device applications, *Sens. Actuators A Phys.*, 233, 2015, 195-201.
26.YAN, J., JEONG, Y.G., High Performance flexible piezoelectric nanogenerators based on $BaTiO_3$ nanofibers in different alignment Modes, *ACS Appl. Mater. Interfaces*, 8(24), 2016, 15700-15709.
27.CASTERA, P., TULLI, D., GUTIERREZ, A.M., SANCHIS, P., Influence of $BaTiO_3$ ferroelectric orientation for electro-optic modulation on silicon, *Opt. Express*, 23(12), 2015, 15332-15342.
28. HE, Y., ZHANG, T., ZHENG, W., WANG, R., LIU, X., XIA, Y., ZHAO, J., Humidity sensing properties of $BaTiO_3$ nanofiber prepared via electrospinning, *Sens. Actuators B-Chem.* 146(1), 2010, 98-102.
29.KAPPADAN, S., GEBREAB, T.W., THOMAS, S., KALARIKKAL, N., Tetragonal $BaTiO_3$ nanoparticles: an efficient photocatalyst for the degradation of organic pollutants, *Mater. Sci. Semicond. Process.*, 51, 2016, 42-47.
30. MA, Z., CAO, C., YUAN, J., LIU, Q., WANG, J., Enhanced microwave absorption of $BaTiO_3$-based ferroelectric/ferromagnetic nanocomposite, *Appl. Surf. Sci.*, 258(19), 2012, 7556-7561.
31.S.A, P., BARBOSA, J., BDIKIN, I., ALMEIDA, B., ROLO, A.G., GOMES, ED.M., BELSLEY, M., KHOLKIN, A.L., ISAKOV, D., Ferroelectric characterization of aligned barium titanate nanofibres, *J. Phys. D Appl. Phys.*, 46(10), 2013.
32. SEAGER, C.H., MCINTYRE, D.C., WARREN, W.L., TUTTLE, B.A., Charge trapping and device behavior in ferroelectric memories, *Appl. Phys. Lett.*, 68(19), 1996, 2660-2662.
33.BAUER, M.J., SNYDER, C.S., BOWLAND, C.C., UHL, A.M., BUDI, M.A.K., VILLANCIO-WOLTER, M., SODANO, H.A., ANDREW, J.S., Structure-property relationships in aligned electrospun barium titanate nanofibers, *J. Am. Ceram. Soc.*, 99(12), 2016, 3902-3908.
34.PETROVSKY, V., PETROVSKY, T., KAMLAPURKAR, S., DOGAN, F., Dielectric constant of barium titanate powders near Curie temperature, *J. Am. Ceram. Soc.*, 91(11), 2008, 3590-3592.
35. KUO, D.-H., CHANG, C.-C., SU, T.-Y., WANG, W.-K., LIN, B.-Y., Dielectric behaviours of multi-doped $BaTiO_3$/epoxy composites, *J. Eur. Ceram. Soc.*, 21(9), 2001, 1171-1177.
36. BELL, A., Grain size effects in barium titanate-revisited, in: *Proceedings of 1994 IEEE International Symposium on Applications of Ferroelectrics, IEEE*, 1994, 14-17.
37.BUESSEM, W.R., CROSS, L.E., GOSWAMI, A.K., Effect of two-dimensional pressure on the permittivity of fine-and coarse-grained barium titanate, *J. Am. Ceram. Soc.*, 75(11), 1992, 2926-2929.
38.TAKEUCHI, T., TABUCHI, M., ADO, K., HONJO, K., NAKAMURA, O., KAGEYAMA, H., SUYAMA, Y., OHTORI, N., NAGASAWA, M., Grain size dependence of dielectric properties of ultrafine $BaTiO_3$ prepared by a sol-crystal method, *J. Mater. Sci.*, 32(15), 1997, 4053-4060.

39. WADA, S., YASUNO, H., HOSHINA, T., NAM, S.-M., KAKEMOTO, H., TSURUMI, T., Preparation of nm-sized barium titanate fine particles and their powder dielectric properties, *Jpn. J. Appl. Phys.*, 42(9S), 2003, 6188.
40. HOSHINA, T., Size effect of barium titanate: fine particles and ceramics, *J. Ceram. Soc. Jpn.*, 121(1410), 2013, 156-161.
41. MOTA, C., LABARDI, M., TROMBI, L., ASTOLFI, L., D'ACUNTO, M., PUPPI, D., GALLONE, G., CHIELLINI, F., BERRETTINI, S., BRUSCHINI, L., DANTI, S., Design, fabrication and characterization of composite piezoelectric ultrafine fibers for cochlear stimulation, *Mater. Des.*, 122, 2017, 206-219. https://doi.org/10.1016/j.matdes.2017.03.013
42. ALLURI, N.R., SARAVANAKUMAR, B., KIM, S.J., Flexible, hybrid piezoelectric film (BaTi(1–x) Zr x O_3)/PVDF nanogenerator as a self-powered fluid velocity sensor, *ACSAppl. Mater. Interfaces*, 7, 2015, 9831-9840. https://doi.org/10.1021/acsami.5b01760
43. SIDDIQUI, S., KIM, D.I., DUY, L.T., NGUYEN, M.T., MUHAMMAD, S., YOON, W.-S., LEE, N.E., High-performance flexible lead-free nanocomposite piezoelectric nanogenerator for bio-mechanical energy harvesting and storage, *Nano Energy*, 15, 2015, 177-185. https://doi.org/10.1016/j.nanoen.2015.04.030
44. SHIN, S.H., KIM, Y.H., LEE, M.H., JUNG, J.Y., NAH, J., Hemispherically aggregated $BaTiO_3$ nanoparticle composite thin film for high-performance flexible piezoelectric nanogenerator, *ACS Nano*, 8, 2014, 2766-2773. https://doi.org/10.1021/nn406481k
45. GENCHI, G.G., MARINO, A., ROCCA, A., MATTOLI, V., CIOFANI, G., Barium titanate nanoparticles:promising multitasking vectors in nanomedicine, *Nanotechnology*, 27, 2016, 232001. https://doi.org/10.1088/0957-4484/27/23/232001.
46. CHO S., LEE, J.S., JANG J. Enhanced crystallinity, dielectric, and energy harvesting performances of surface-treated barium titanate hollow nanospheres/PVDF nanocomposites, *Adv. Mater. Interfaces*, 2, 2015, 1500098. https://doi.org/10.1002/admi.201500098
47. SUN, L., SHI, Z., LIANG, L., WEI, S., WANG, H., DASTAN, D., SUNC, K., FAN, R., Layer-structured $BaTiO_3$/P(VDF–HFP) composites with concurrently improved dielectric permittivity and breakdown strength toward capacitive energy-storage applications, *Journal of Materials Chemistry C*, 30, 2020.
48. ZHOU, J., GOU, X., FAN, D., WANG, J., WAN, Z. Polydimethylsiloxane/$BaTiO_3$ Nanogenerators with a Surface-Assembled Mosaic Structure for Enhanced Piezoelectric Sensing, *ACS Appl. Mater. Interfaces*, 14(33), 2022, 38105-38115.
49. MEISAK, D., KINKA, M., PLYUSHCH, A., MACUTKEVIČ, J., ZARKOV, A., SCHAEFER, S., SELSKIS, A., SAMULIONIS, V., KUZHIR P., BANYS, J., FIERRO, V. and CELZARD A. Piezoelectric Nanogenerators Based on $BaTiO_3$/PDMS Composites for High-Frequency Applications, *ACS Omega*, 8(15), 2023, 13911-13919.
50. HUANXIN, S.A, XIAOBING, W.A, CHAOYUE, L.A, ZIFA, W.B, YONGHUI, W.A, JIAWEI, ZHANG A., ZHANG A., CHUNLIN, Z.C., JIAGANG, WU C, HAIWU, Z. Enhanced energy harvesting ability of polydimethylsiloxane-$BaTiO_3$-based flexible piezoelectric nanogenerator for tactile imitation application, *Nano Energy*, 83, 2021, 105809.
51. BOUHAMED, A., JÖHRMANN N., NAIFAR S., BÖHM B., HELLWIG O., WUNDERLE B., KANOUN O., Collaborative Filler Network for Enhancing the Performance of BaTiO3/PDMS Flexible Piezoelectric Polymer Composite Nanogenerators, *Sensors*, 22(11), 2022, 10.3390/s22114181.
52. https://www.novocontrol.de/php/turn_key_10_90.php
53. MAJID, N., BEREAN, K., SIVACARENDRAN, B., CNT/PDMS composite membranes for H_2 and CH_4 gas separation, *Int. J. Hydrogen Energy*, 38, 2013, 10494.
54. XUE, I., ZHANG, I., HAN, Y., Study of hydrophilicity and stability of chemically modified PDMS surface using piranha and KOH solution, *Surf. Interface Anal*, 44, 2012, 62.
55. MAJID, N., BEREANAD, K., CNT/PDMS composite membranes for H_2 and CH_4 gas separation, *Int. J. Hydrogen Energy*, 38, 2013, 10494.

56.RAHIMPOUR, A., MADAENI, S.S., ZERESHKI, S., MANSOURPANAH, Y., Preparation and characterization of modified nano-porous PVDF membrane with high antifouling property using UV photo-grafting, *Appl. Surf. Sci.* 255, 2009, 7455.
57.CHINAGLIA, D.L., Influence of the solvent evaporation rate on the crystalline phases of solution-cast poly (vinylidene fluoride) films, *J. Appl. Pol. Sci.*, 2. 2010,116.
58.ABRAHAM, F.F., Orientation order of dipole molecules in the surface of embryonic droplets, *Science*, 168, 1970, 833-5.
59.GREGORIO, J.R., CESTARI, M., Effect of crystallization temperature on the crystalline phase content and morphology of poly (vinylidene fluoride), *J. Polym. Sci. B*, 32, 1994, 859
60.GREGORIO, F.R., LANCEROS-MENDEZ, S., Processing and characterization of a novel nonporous poly (vinilidene fluoride) films in the β phase, J Non Cryst Solids (2006) 352, 2226
61.FALKAND, M., KNOP, O., *Water: a comprehensive treatise*, Franks F., Plenum, New York, 2, 1973, 55.
62.WEI, W., DA'AN, L., QINHUI, Z., YAOYAO, Z., JIAO, D.L., XIANGYONG Z., HAOSU, L., Shear-mode piezoelectric properties of ternary PbIn1/2 Nb1/2 O3 – PbMg1/3 Nb2/3 O 3 – PbTiO3 single crystals, *Journal of applied physics* 107, 084101, 2010
63.*** https://www.novocontrol.de/newsletter/DNL16.PDF
64.LI THENG, L., AMBRI, M., ISKANDAR, Y., HIROSHI, M., Comparison of piezoelectric energy harvesting performance using silicon and graphene cantilever beam, *Microsystem Technologies*, 24(1), 2018
65.***https://www.ni.com/ro-ro/shop/labview.html

Manuscript received: 08.08.2023